Spectroscopy 17 (2003) 139–159
IOS Press

Tracking chemical changes in a live cell: Biomedical applications of SR-FTIR spectromicroscopy

Hoi-Ying N. Holman *, Michael C. Martin and Wayne R. McKinney
Lawrence Berkeley National Lab, Berkeley, CA 94720, USA

Abstract. Synchrotron radiation-based Fourier transform infrared (SR-FTIR) spectromicroscopy is a newly emerging bioanalytical and imaging tool. This unique technique provides mid-infrared (IR) spectra, hence chemical information, with high signal-to-noise at spatial resolutions as fine as 3 to 10 microns. Thus it enables researchers to locate, identify, and track specific chemical events within an individual living mammalian cell. Mid-IR photons are too low in energy (0.05–0.5 eV) to either break bonds or to cause ionization. In this review, we show that the synchrotron IR beam has no detectable effects on the short- and long-term viability, reproductive integrity, cell-cycle progression, and mitochondrial metabolism in living human cells, and produces only minimal sample heating ($<0.5^{\circ}$C). We will then present several examples demonstrating the application potentials of SR-FTIR spectromicroscopy in biomedical research. These will include monitoring living cells progressing through the cell cycle, including death, and cells reacting to dilute concentrations of toxins.

1. Introduction

Diseases usually begin with a single cell. With the continuing successes in gene sequencing and protein identification, biomedical researchers are now increasingly focused on understanding the onset of disease and the functions of diseased cells. This necessitates a more thorough comprehension of the interactions of living cells with their surrounding tissues and micro-environments. Imaging techniques which can simultaneously provide morphological and chemical information within living cells and tissues are very powerful unifying tools for meeting this scientific need. Today intensive research in experimental biology, spectroscopy, and analytical instrumentation is seeking new ways to image chemical information within living cells.

Infrared (IR) spectromicroscopy combines infrared spectroscopy, a sensitive analytical chemistry technique, with microscopy to enable detailed chemical analysis on a microscopic scale. Many common biomolecules, such as nucleic acids, proteins, and lipids have characteristic and well-defined IR-active vibrational modes [46,61,71]. With appropriate interpretation of measured IR spectra one can detect, identify, and quantify many molecular species within a biological sample. This IR spectroscopy capability has been combined with microscopy, which allows one to conduct chemical analysis and map the distribution of chemical species with fine spatial resolution. The resultant spectromicroscopy technique applied to biological systems has been reviewed many times, recently in *Science* [84].

Sufficient signal to noise for detailed spectral interpretation of samples the size of individual human cells has only been very recently achieved by adding the brightness of synchrotron-based IR sources

*Corresponding author: Hoi-Ying N. Holman, Mail Stop 70A-3317, Lawrence Berkeley National Lab, Berkeley, CA 94720, USA. Tel.: +1 510 486 5943; Fax: +1 510 486 7152; E-mail: HYHolman@lbl.gov.

to the technique [13,65]. Fourier transform infrared (FTIR) spectromicroscopy with a synchrotron radiation-based (SR) source is a newly emerging bioanalytical and imaging tool that can monitor biochemical events within different compartments of an individual living cell without the need for fixing, staining, or labeling. Recent uses of synchrotron infrared spectromicroscopy include the examination of biological samples such as individual living cells [32–34,37,38,51,83], tissue samples [11,19,53,54], microbial–chemical interactions in environmental settings [28,31], protein conformations [52,87], and plant-soil interactions [64].

In this review paper we will describe the SR-FTIR spectromicroscopy technique, demonstrate that this technique is a truly non-destructive chemical microprobe, and review examples demonstrating the potential applications of this novel technique for biomedical research. All the measurements presented here were performed at the Advanced Light Source (ALS) Beamline 1.4 at Lawrence Berkeley National Laboratory [47,49,50].

2. Synchrotron FTIR spectromicroscopy

Conventional mid-infrared sources used in FTIR instruments are thermal emission elements that produce a graybody spectrum from a filament heated to 1000 to 2000 K. These elements are physically large (at least several millimeters), and typically radiate in all directions. The optics of the FTIR bench collect the light, then collimate and pass it through the scanning interferometer. Next, this modulated light is sent into the IR microscope. The IR microscope objective and condenser optics are all-reflective and focus the IR light to a small spot on a sample. Finally, the light that the sample reflects or transmits is collected, focused onto an appropriate infrared detector, and processed by a computer via a Fourier transform to produce an infrared spectrum.

The brightness (flux/area/solid angle) attainable in IR spectromicroscopy is governed primarily by how closely the source approximates a point. The thermal emission sources can be focused down to 75 to 100 μm with an IR microscope. To measure something smaller, you must mask away part of the incoming light, significantly reducing the signal strength. A true point source could be focused to a diffraction-limited spot size; with f/1 optics this is approximately the wavelength of the light [15]. This is where using a synchrotron as an IR source makes a big improvement.

A synchrotron is a high-energy electron storage ring optimized for the production and collection of the intense light radiated by the electrons upon acceleration. In the mid-IR wavelengths – 3 to 20 μm – the effective source size for a typical synchrotron light source is nearly diffraction-limited. In other words, it is very close to an ideal point source. This means that in FTIR spectromicroscopy based on synchrotron radiation (SR), the beam is focused to a spot with a diameter $\leqslant$10 μm [14,15,47], smaller than a typical mammalian cell. This provides hundreds of times the brightness of conventional IR sources. The sample can be positioned using a computer-controlled x–y–z stage with 1-μm precision, allowing mapping measurements of FTIR spectra as a function of x and y position on the sample. A schematic of a synchrotron infrared beamline is shown in Fig. 1. This considerably higher brightness available at synchrotron IR spectromicroscopy facilities enables a multitude of new scientific applications where size matters.

The high brightness of the synchrotron IR source plays an important role in studying localized biochemical phenomena in a living single cell. To demonstrate the advantage of using a synchrotron source, we compare the measured signal to noise ratio in the mid-IR for a conventional thermal IR source and the synchrotron. These measurements were made using a Thermo Nicolet Nexus 870 FTIR bench and

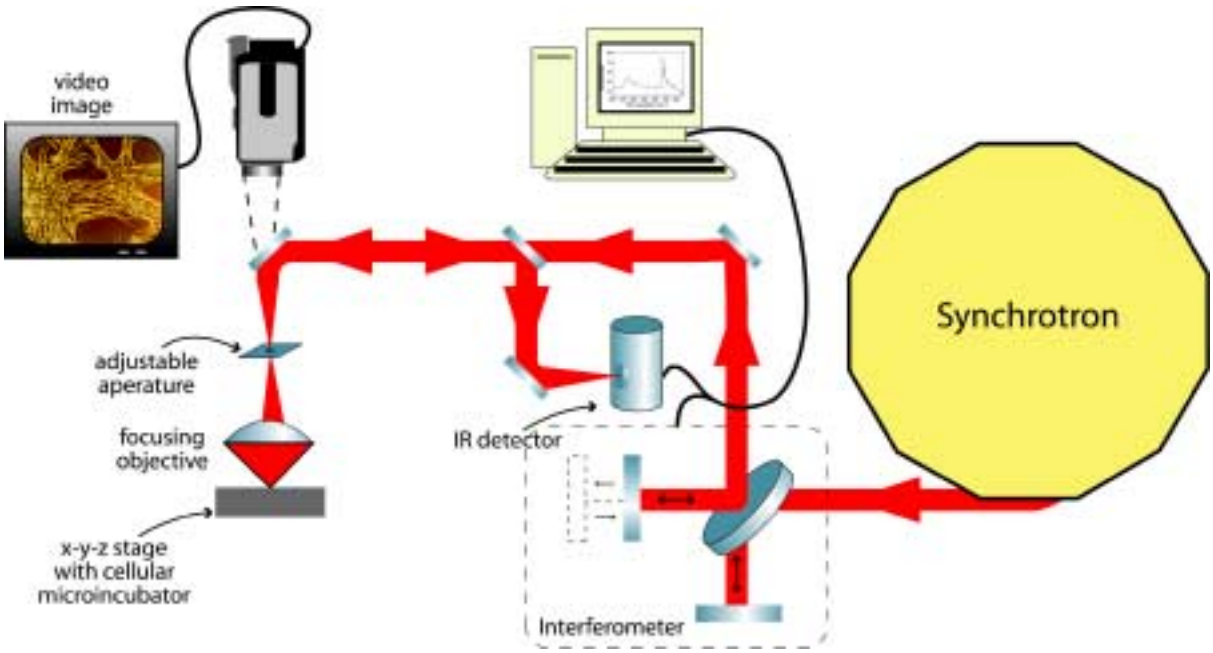

Fig. 1. Schematic diagram of synchrotron-based FTIR spectromicroscopy experimental setup. Synchrotron radiation from a bending magnet is collected, collimated, and transported to a commercial FTIR interferometer bench. After modulation by the interferometer, a commercial infrared microscope focuses the beam onto the sample with all-reflecting optics. Biological samples can be placed in an on-stage mini-incubator with environmental controls. The stage is computer controlled and rasters the sample in the x–y plane to ± 1 μm precision to obtain spectral maps across the sample. The light reflected from the sample is collected by the same microscope optics and sent to an IR detector. A computer performs a Fourier transform on the measured interferogram to obtain an infrared spectrum.

a Thermo SpectraTech Contiuμm IR microscope at the ALS Beamline 1.4. We measured 100% reflection lines utilizing a gold-coated glass sample for both sources and for various aperture sizes. We used an MCT-B detector, co-added 128 scans for background and sample measurements at a spectral resolution of 4 cm^{-1} and a scanning mirror velocity of 1.8988 cm/sec. The top panel of Fig. 2 compares the measured 100% lines for a 10×10 micron aperture for the EverGlo^{TM} thermal IR source and the synchrotron source. As noted in the figure, the RMS noise value determined between 2450 and 2550 cm^{-1} is significantly better for the synchrotron source.

The signal-to-noise value at 2500 cm^{-1} was obtained for each source and aperture setting measured by dividing the single beam intensity at this wavenumber value by the corresponding RMS noise value. The results are also plotted on a log scale in Fig. 2. The signal to noise ratio for the thermal EverGlo^{TM} source drops rapidly as the aperture size decreases, whereas for the synchrotron source the signal to noise ratio remains essentially unchanged until the aperture size finally reaches the beam spot size of 10 microns. Since the focused size of the thermal IR source is greater than 70×70 microns, closing down the aperture size simply reduces the total IR signal proportional to the area reduction. The noise level becomes significantly worse as the aperture is size is decreased, becoming essentially unusable at aperture sizes below 20×20 microns.

The focused spot size of the synchrotron source, however, is diffraction limited (3 to 10 microns in diameter) so its signal to noise ratio is only affected at aperture sizes smaller than 10 microns. As shown in the lower panel of Fig. 2, the synchrotron is observed to have a better signal to noise than the thermal

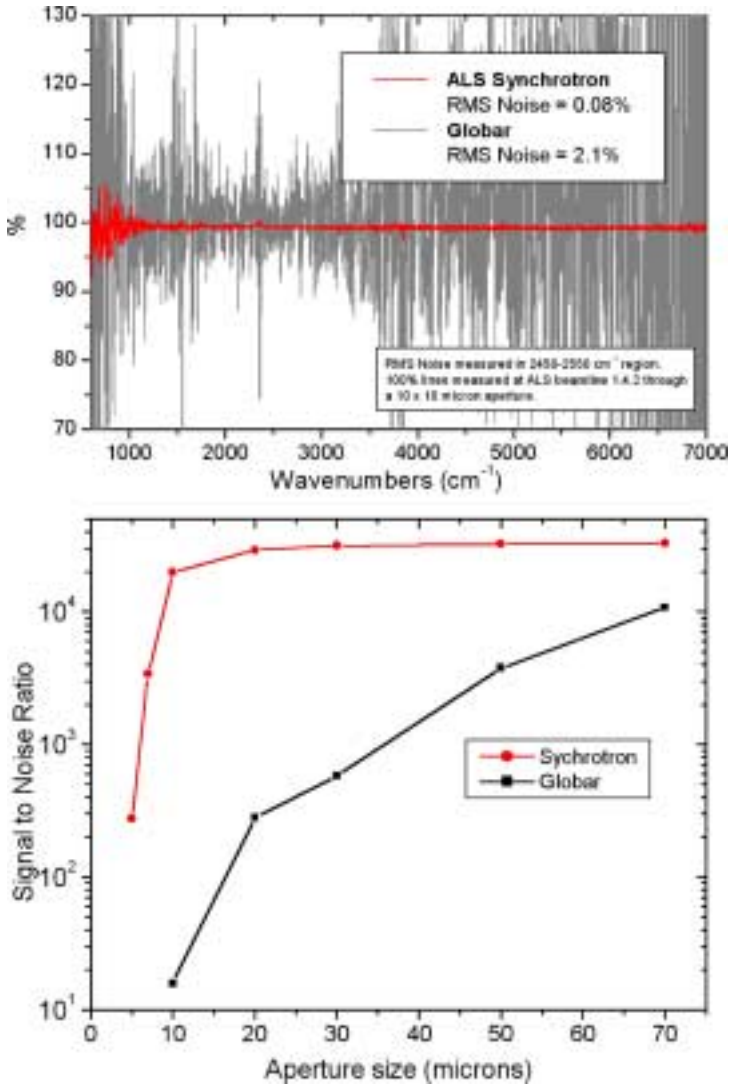

Fig. 2. Comparison of measured noise around 100% reflectance for the thermal and synchrotron IR sources with a 10×10 micron aperture (upper panel). Signal to noise ratio on a log scale as a function of aperture size for the synchrotron and thermal IR sources (lower panel). The synchrotron source extends FTIR spectromicroscopy to below 20 micron spatial resolution with a signal to noise advantage over conventional IR sources of at least 1000.

IR source at all aperture sizes. The noise doesn't start to increase until the aperture size reaches 10×10 microns, and a usable signal is maintained even at the smallest aperture sizes available of 5×5 microns. Note that the longest wavelengths (lower wavenumbers) are being cutoff by the smallest aperture settings as is expected by the diffraction limited spot sizes (approximately the wavelength).

Since the synchrotron source's signal to noise ratio is more than 1000 times better than the thermal source for spatial resolutions of 3 to 10 microns, this technique is ideal for the study of small and/or heterogeneous samples, for example; individual living cells, microorganisms, and larger biological systems in which local biochemistry may have significant spatial variations.

3. Truly non-destructive nature of SR-FTIR spectromicroscopy

Non-destructive in the context of cellular micro-imaging has become an imprecise and relative term. It can merely mean that the sample was so rapidly frozen that changes are thought to minimal. Of course in these cases the cell is no longer living. Recently even two-photon fluorescence [23,41,70,75], which uses lower energy photons than traditional UV fluorescence, has been linked to apoptosis-like cell death [75]. Because of this ambiguity, we have performed a series of tests to explicitly quantify the non-destructive properties of SR-FTIR spectromicroscopy.

Mid-infrared photons are significantly lower in energy (0.05–0.5 eV) than the excitation sources used in fluorescence probes including the newer two-photon techniques (photons energies of approximately 1 eV), implying that photo-induced effects will be minimal. Although mid-IR photons are too low in energy to directly break bonds or cause ionization, other effects from the SR-IR source may occur, including sample heating, drying, or other more subtle interactions which could influence long-term metabolic and other cellular physiological processes.

The following highlights the results of *in vitro* studies to determine if the SR-IR beam causes any detectable effects on living cells [35]. Two classes of effects were measured in this study: (1) immediate and/or short-term effects in cell viability, cell-cycle progression, cell metabolism, and (2) long-term effects on the proliferative/metabolic capacity of exposed cells. Four widely accepted cellular and molecular assays were selected to measure these potentially deleterious effects on cells subjected to different doses of the SR-IR beam. Next, infrared spectra were also recorded for exposed and non-exposed cells, and were compared in detail to identify possible immediate chemical changes as a result of exposure to the SR-IR beam. Finally, we determined the steady-state temperature rise in a typical biological sample continuously illuminated by the SR-IR beam.

A human T-1 cell-line from an established aneuploid cell-line derived from human kidney tissue was used in this study [78]. They were selected partly because of their high plating efficiency ($>$90%), and partly because they have been previously used as a model biological system in studies of the effects of radiation and oxygen on human cells [2,5–8]. Most importantly the size of T-1 cells is typically $\sim$10 microns in the G_0 and G_1 phases, which is similar to the size of the synchrotron IR beam.

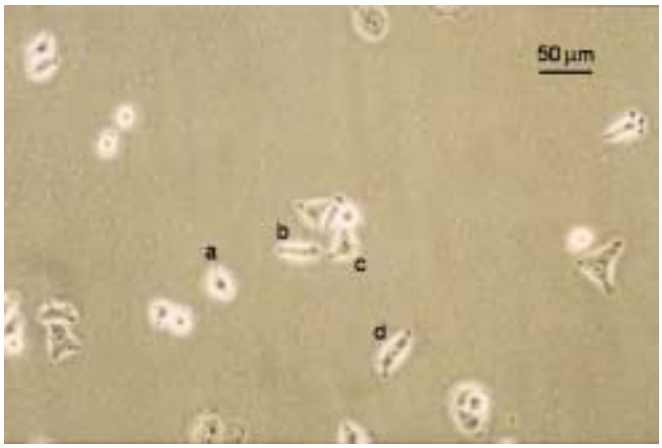

Fig. 3. Photograph showing results from Alcian blue assays of cells exposed to the SR-IR beam for (a) 5 minutes, (b) and (c) 10 minutes, and (d) 20 minutes. Other cells in the field were not exposed and were used as negative controls. No cells show retention of the blue dye demonstrating that no immediate cytotoxicity is observed.

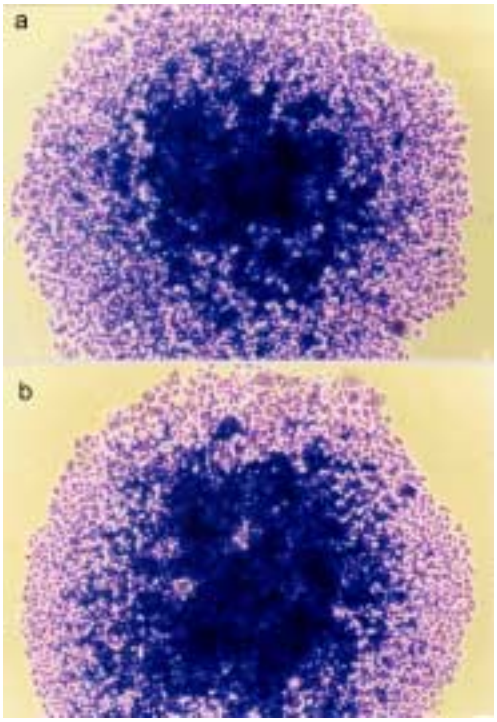

Fig. 4. Photographs showing typical results for colony forming from (a) a negative control cell and (b) a test cell that had been exposed to the SR-IR beam for 20 minutes. Both cells proliferated into similar sized colonies after 10 days.

A custom on-stage mini-incubator was used to maintain the proper moisture and growth environment for the cells while allowing *in situ* SR-FTIR spectromicroscopy measurements. The mini-incubator was temperature controlled via circulating water from a water bath, and infrared transparent CaF_2 windows on the top cover were separately temperature-controlled to avoid condensation. The location of the synchrotron infrared beam within the field of the microscope was fiducialized to approximately one micron by mapping a titanium on silicon calibration target [74]. Every exposure experiment was conducted at 37°C and lasted for less than one hour. Complete experimental details are found in reference [35].

We employed the Alcian blue dye exclusion assay to measure short-term cell viability [88]. As shown in Fig. 3, neither cells exposed to up to 20 minutes of synchrotron IR beam nor nearby non-exposed cells retained the blue dye 6 hours after exposure. This indicates that the SR-IR beam did not produce detectable effects on the viability of exposed cells. Other exposed cells remained free of stain 12 and 24 hours after exposure indicating that their membranes still remained intact.

While the aforementioned short-term test has revealed that cells were active at the time of the Alcian blue assay, the long-term colony-forming assay demonstrates that the exposed cells also continue to proliferate into colonies. The exposed test cells and nearby non-exposed cells proliferated into colonies of similar size (Fig. 4), well over fifty cells in ten days. Since none of the 46 SR-IR exposed test cells developed into colonies with less than 50 cells, we interpret this as an indication that SR-IR beam does not impact cell survival and proliferative activities.

A two-antibody bromodeoxyuridine (BrdU) assay was designed to specifically answer the question, “Do SR-IR beam exposed cells progress into S-phase at the same time as unexposed control cells?” Cell-cycle progression in exposed cells were monitored by the incorporation of BrdU into newly synthesized

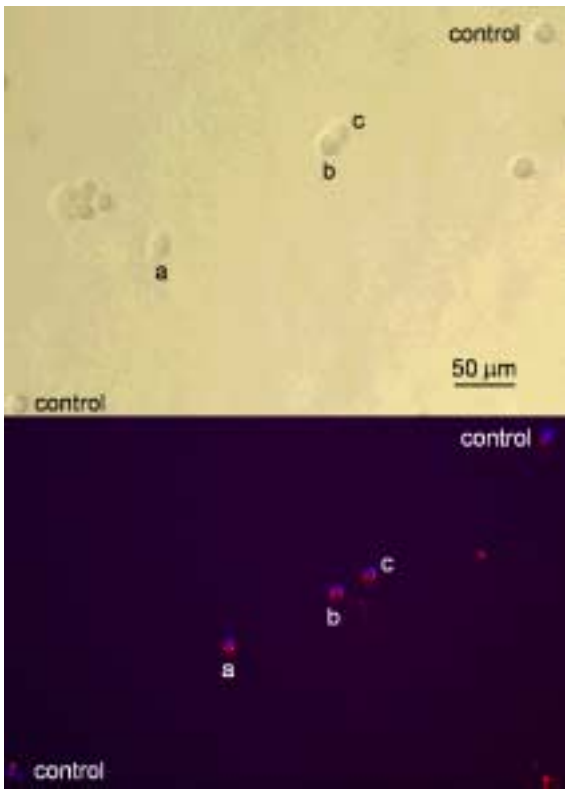

Fig. 5. Photographs showing BrdU assay results for cells exposed to the SR-IR beam for (a) 5 minutes, (b) 10 minutes, and (c) 20 minutes. Two other cells in the field were unexposed and used as negative controls. In the lower panel, the blue color indicates DNA and the red color indicates BrdU incorporation during DNA synthesis. All test and control cells show the same incorporation of BrdU into the DNA.

DNA at 11 hours after cell setup and 10 hours post SR-IR exposure. Both exposed cells and non-exposed controls had reached the DNA synthetic phase (S-phase) of cell-cycle at this 12-hour observation point. For example, the upper photo in Fig. 5 shows an image of 5-, 10-, or 20-minute exposed cells and their neighboring non-exposed controls. The lower photo in Fig. 5 shows that all three exposed cells as well as the controls have incorporated BrdU into the DNA, which is identified by the double color labeling of red for BrdU and blue for DNA. The similarities among these immunofluorescent staining of BrdU and DAPI (4,6-diamidino-2-phenylindole) labeled cells indicate that the exposed cells are not compromised in their ability to enter their S-phase in the cell cycle after exposure to the SR-IR beam. Furthermore, the lack of detectable uptake of BrdU into DNA in exposed and control cells at 6 or 24 hours after their release demonstrates that the cell-cycle progression of SR-IR exposed cells remains uninterrupted.

We have shown that the cell cycle progresses uninterrupted, and now use a MTT (3-[4,5-dimethylthiazol-2-yl]-2,5-diphenyltetrazolium bromide) assay to test for any SR-IR beam effect on ATP and NAD^+-associated metabolic activity. Representative photos of the results are shown in Fig. 6. Cells exposed for 20 minutes and nearby non-exposed controls show similar purple-blue stain. Results were identical for 5- and 10-minute exposures. This implies that both the exposed and negative control cells produced mitochondrial dehydrogenases during the two-hour MTT assay. Mitochondrial dehydrogenases are associated with the ubiquitous metabolic pathway of glycolysis [69] that generates the critical bio-

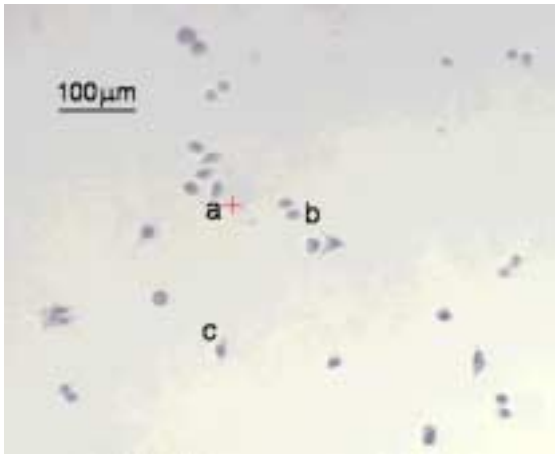

Fig. 6. Photograph showing typical MTT assay results for control and test cells that had been exposed to the SR-IR beam for (a) 5 minutes, (b) 10 minutes, and (c) 20 minutes. Other cells in the field were unexposed and are used as controls. All test and control cells show the same blue color indicating the same level of metabolic activity.

molecules of ATP and NAD^+. These results indicate that the SR-IR beam has negligible effects on this important metabolic pathway which provides energy to cells.

We next compared SR-FTIR spectra of cells as a function of time looking for any biochemical changes induced by the beam. SR-FTIR measurements performed repeatedly on one living cell every 10 minutes for thirty minutes showed an unchanging IR spectrum to within 0.005 absorbance units across the entire mid-IR spectral range. Longer exposure times can be tested, however the living cell continues growing through its cell cycle, which results in other spectral changes as described below [34].

In all 5 assays studied (Alcian blue, colony formation, BrdU, MTT, and SR-IR spectra) we found no detectable changes between cells exposed for 5, 10, and 20 minutes to the synchrotron infrared beam and nearby non-exposed controls. 267 individual cells were tested using standard biochemical assays with zero tests showing any measurable cytotoxic effects (counting statistics error is 6.1%), with over 1000 control cells used. Additionally, infrared spectra that are a measure of the overall biochemistry within a cell were obtained from test and control cells, and showed no spectral changes. These results show that the high-brightness mid-IR synchrotron beam is not only non-destructive, but also causes no effects on both the short- and long-term viability, proliferation, and metabolism within living human T-1 cells. Although the present study has focused on only one established human cell line, we anticipate that these results will be generally applicable to most, if not all, living biological systems.

We have shown that synchrotron-based IR spectromicroscopy induces no detectable effects to cellular viability, reproductive integrity, cell-cycle progression, or metabolic activity when exposed to this beam. The power levels in the mid-IR spectral region of the SR beam are generally fairly low ($\sim$1 mW integrated power [35]). However, since all cellular processes are sensitive to temperature, we must determine the extent of heating by the intense synchrotron beam.

The phospholipid dipalmitoylphosphatidylcholine (DPPC) was utilized as an internal thermometer to determine the steady state temperature rise due to the continuous exposure to the SR-IR beam [48]. DPPC, when dispersed in water, forms bilayers which exist in at least two different states, depending on the temperature. These states are separated by a phase transition temperature (T_m) at around 315 K, when the bilayers are converted from a gel into a liquid–crystalline state [39,67].

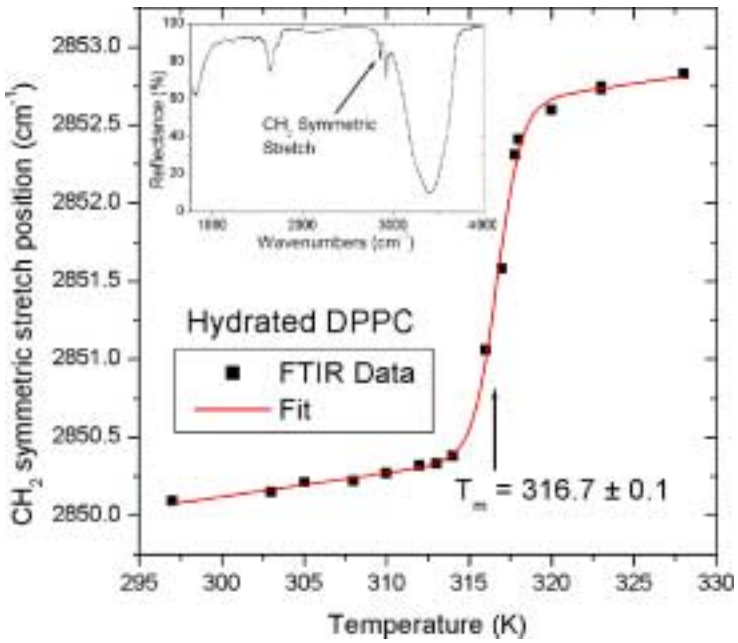

Fig. 7. Plot of the measured CH_2 symmetric stretch mode center frequency as a function of temperature. Data was obtained as the temperature was raised and lowered. The solid line is a best fit to the data using a Boltzman function with a linear background. (Inset) Infrared reflectance spectrum of hydrated DPPC at $T = 328$ K which is above the melting transition temperature, T_m. The largest absorptions are due to water, and the CH_2 symmetric stretch vibrational mode around 2850 cm^{-1} used as a temperature probe in this study is labeled.

Mid-IR spectra were obtained at 4 cm^{-1} resolution with a Thermo Nicolet Magna 760 FTIR bench connected to a Nic-Plan IR microscope. A Ge-coated KBr beamsplitter and liquid nitrogen cooled MCT-A detector were used and data was collected in reflection geometry covering the 800–6000 cm^{-1} spectral region. Samples were mounted on an MMR Technologies optical transmission micro-miniature refrigerator/heater fitted with KRS-5 windows for IR transparency. The sample temperature was set and monitored by an MMR K-20 programmable temperature controller to within an accuracy of 0.1 K.

A 20 : 1 dilution of the hydrated DPPC dispersion was placed on a gold-coated piece of glass, and a CaF_2 window was used to cover the sample creating a uniform layer thickness. Vacuum grease was carefully applied to the edges of the CaF_2 window to ensure the sample was sealed inside and no water loss during heating would occur. This sample was then mounted onto the temperature finger of the MMR heater/cooler with thermal grease. Measured reflectance spectra were ratioed to a background spectrum obtained with the same CaF_2 window on gold but without the DPPC present.

The inset to Fig. 7 shows the measured infrared spectrum of the hydrated DPPC at $T = 328$ K (above T_m). As has been shown before [39,67], the methylene (CH_2) symmetric stretch vibration at around 2850 cm^{-1} and the phosphate asymmetric stretching mode around 1240 cm^{-1} shift when the sample passes through the phase transition. For this study we monitored the CH_2 symmetric stretch mode (labeled in Fig. 7).

The CH_2 symmetric stretch mode's center frequency was measured using the less bright thermal Globar^{TM} IR source as the sample temperature was increased and decreased through T_m. The results are displayed in main part of Fig. 4 along with a best fit to the data using a Boltzman expression with a linear background. The transition temperature was determined by this fit to be $T_m = 316.7 \pm 0.1$ K.

To test if the more concentrated flux of the synchrotron source causes any local sample heating, we set the sample temperature to be continuously held at 317.0 K. This temperature setting is where we would have maximum sensitivity to temperature changes as it is the point of greatest slope in Fig. 7. The IR source was then switched to the brighter synchrotron source and infrared spectra were acquired every minute for 30 minutes to look for any heating that occurred instantaneously or more slowly over time. The temperature of the sample within the beam spot was measured by monitoring the position of the CH_2 symmetric stretch mode as previously calibrated. The sample temperature fluctuated slightly over the 30 minutes, however no discernable longer-term trends were observed.

Statistical analysis of the measured temperature fluctuations determined that the average temperature rise due to the SR beam is a very modest 0.5 ± 0.2 K. We therefore conclude that the synchrotron IR source does not appreciably heat the sample under investigation. Since the test sample is mainly water, 98% by weight, we are confident that our result generalizes to most biological samples.

Thus, the term non-destructive is truly appropriate for SR-FTIR spectromicroscopy.

4. Cell cycle and cell death

As a first evaluation of the potential of the SR-FTIR spectromicroscopy technique to image changes within a single living cell, we investigated the changes in infrared spectral features as individual human cells progressed through their cell cycle, and finally into death. The normal human fetal lung fibroblast IMR-90 P4 (passage 4) cell line of female origin was used for this study [58]. Grown to confluency, the cells are $\sim$82% synchronized into the G_1 phase as determined by fluorescence-activated cell sorting (FACS) [18,20,21].

The cells were placed on gold coated glass slides which were inserted into a small chilled chamber with a thin ($\sim$0.5 mm) IR-transparent ZnSe window to maintain a more constant humidity, and prolong cell viability. Data for this study was acquired in the double-pass reflection/transmission mode (the IR beam passes through a cell and is reflected back from the gold surface through the cell again). The sample stage was moved to align the center of the cell of interest with the focused SR-IR spot to within a few microns. Typically spectra were obtained from an individual cell using 4 cm^{-1} resolution and 64 co-added interferograms. On the order of 100 individual cells were measured, spread through the various morphologies. No apertures were used in the beam from the source to the sample, therefore the nearly diffraction limited spot size in the mid-IR region of interest was always ten microns or less.

We found that cells identified as being in the G_1, S and G_2/M parts of the cycle showed clearly different spectra. Fig. 8 shows the 1800 to 900 cm^{-1} region for typical individual cells in each of these three phases. These spectra are not normalized. Cell to cell spectral variations within each cell cycle phase were significantly smaller than the phase to phase changes reported here. During S phase the DNA is undergoing replication and we observe that the absorptions in the DNA/RNA spectral region increase relative to the G_1 phase spectra by approximately a factor of two.

When a G_2/M phase cell is measured we observe a large increase in the overall absorbance (uppermost spectrum in Fig. 8). This may be a result of more material in the cell, or because the thickness may be different in the M phase. In the second case there could be a greater path-length for the IR beam to traverse. Other more complicated mechanisms may also be active including the condensation of chromatin during these phases of the cell cycle. Absorptions in the DNA/RNA region are significantly increased relative to the protein peaks. It is also noteworthy that the peak around 1395 cm^{-1} is noticeably larger in the G_2/M phase than in the other phases.

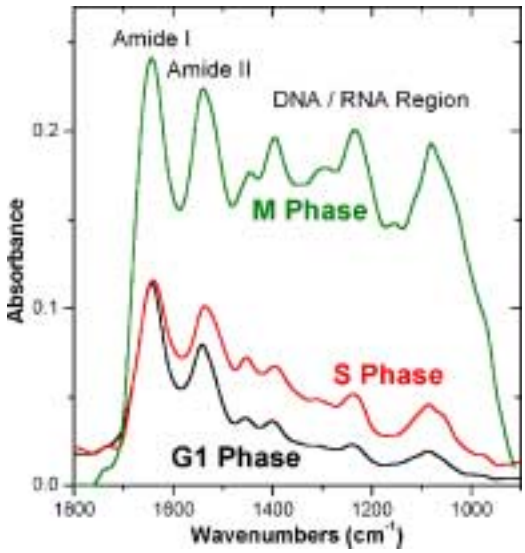

Fig. 8. IR spectra of individual cells in different stages of the cell cycle. Spectra were not normalized, but a linear baseline was subtracted over the range of 2000 to 650 cm^{-1}.

A previous study has looked at the average infrared absorption response of human myeloid leukemia cells, separated into G_1, S and G_2 cell cycle stages by centrifugal elutriation, either macroscopically by measuring $\sim 10^4$ cells or microscopically by averaging the response of 10–50 individual cells measured using a conventional IR source and a 15 μm aperture in an IR microscope [10,24]. They were unable to separate and measure cells in the M phase due to the short time their cells spend in that phase ($<$4% of the cell division cycle is in M phase). Our G1 and S phase results in Fig. 8 (each from a single cell) confirm conventional IR measurements of Boydston-White et al. [10,24]. We observe the intensity of the DNA/RNA spectral region peaks relative to the protein Amide peak intensities increase markedly in S phase compared to G_1 phase. Since the DNA is being replicated throughout S phase is it reasonable to expect a greater DNA signal in the IR spectra. Alternatively, Boydston-White et al. hypothesize that in the G phases the DNA is packed so tightly into nucleosomes that the IR absorptions are optically thick and will therefore be unobservable in the IR spectra. However, during the S phase portions of the DNA are packed less densely and therefore will contribute to the IR spectrum [10,24]. In our S phase spectrum the PO_2^- peak at $\sim$1085 cm^{-1} shows a small "nose" consistent with the spectrum of RNA [10,77]. Further studies are necessary to fully assess whether DNA/RNA packing and/or content is responsible for the increased IR absorption observed.

The centroid positions of the protein amide I and II peaks were observed to shift to lower energy in the S phase compared to the G_1 phase. Using a simple amide peak shape interpretation, these shifts are consistent with more cellular proteins having β-sheet secondary structure in the S phase compared to a higher α-helix protein content in G_1 phase [12,30,46,71,72].

The uppermost trace in Fig. 8 is significantly different than the G_1 or S phase spectra. Boydston-White et al. [10,24] showed that their G_2 phase cells had a very similar spectra to those in the G_1 phase. Therefore one can conclude that the measured cell was in the M phase and not in the G_2 phase. To our knowledge, the top curve in Fig. 8 presents the first measured M phase IR spectrum from a mitotic cell. The overall absorption intensity in the DNA/RNA spectral region increased significantly relative to the protein amide vibration peaks. Since the DNA is most tightly packed into chromosomes during M phase

[3], the optical density arguments of Boydston-White et al. [10,24] would point toward this enhancement being due to RNA in the cell. Since the nucleolus disappears during mitosis with the presumed dispersal of the associated RNA and ribosomes a straightforward interpretation would be that the dispersed RNA is now optically thinner and contributes more to the IR spectrum. However, the ratio of the $\sim$1085 cm^{-1} PO_2^- to $\sim$1230 cm^{-1} phosphodiester and amide III peaks is closer to that of DNA. The full understanding of this complex behavior will require further study and interpretation.

The M phase spectrum also shows the absorption mode at $\sim$1395 cm^{-1} is much enhanced compared to the G_1 and S phase spectra. As this one peak grows much more than the overall protein, DNA/RNA, or lipid (not shown) spectral regions, one can conclude that this growth is not simply related to the amount or density of these major cellular components. Since absorptions affected by helical conformations of DNA as well as protein side chain vibrations are components to this spectral region [45], future detailed experiments will be required to assign this intensity growth to a specific phenomenon.

Occasionally some cells exhibited different spectral characteristics near the protein amide I and II peaks even though the cells were morphologically identical. Comparing these spectra to published research on lysed necrotic cells [38] we see that the spectral changes observed indicate that the cells were dying or already dead. The spectrum of one such cell is shown in Fig. 9 along with the spectrum of a normal living G_1 phase cell. The "dying" cell shows two characteristic spectral signatures indicative of death [38]. First, the centroids of the protein amide I and II peaks shift from 1644 to 1633 and from 1542 to 1531 cm^{-1}, respectively, indicating a change in the overall protein conformational states within the cell. Second, we observe the appearance of a peak around 1743 cm^{-1}.

We also measured a number of cells that were visually seen to have non-intact cell membranes. Spectra from these cells were similar to those reported by Jamin et al. [38] in that a peak at $\sim$ 1728 cm^{-1} became prominent with a shoulder at $\sim$1743 cm^{-1}. The amide peaks were also observed to shift down to lower energies with the exact amount of the shifts varying from cell to cell.

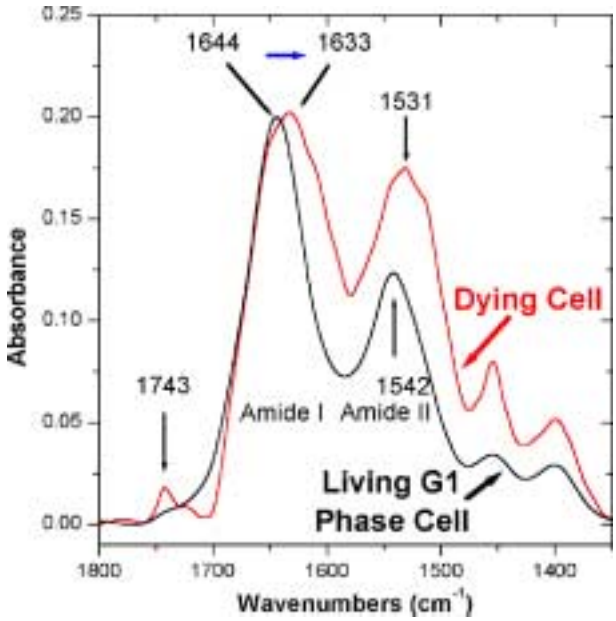

Fig. 9. IR spectra comparison of individual living and dying cells. Spectra were normalized to the amide I peak, and a linear baseline was subtracted from 1800 to 1350 cm^{-1}.

As a first (overly simplistic) analysis we fitted the amide I peak shape in the living and dying cell spectra to a series of empirically determined peak positions for the various secondary structures of proteins [12,30,46,71,72]. When we compare the amplitudes of the three nominal "β-sheet" subcomponents at 1605, 1623, and 1667 cm^{-1} to the central α-helix component at 1640 cm^{-1}, we find that the amount of "β-sheet" secondary structures increases by $\sim$20% in the dying cell compared to the living cell. The amount of "random coils" is only increased by $\sim$2% in the dying cell. These structural changes in the cellular proteins could be due to a different distribution of proteins during apoptosis, or to denaturation of the existing proteins. This analysis is simplistic and ignores other spectral features under the amide I envelope such as ring breathing and C=O stretching vibrations of DNA and RNA. Furthermore, Torii and Tasumi [76] have demonstrated that the interpretation of amide I envelopes requires more than simple deconvolution with spectral features from a "basis set" of model proteins. Their analysis of the IR spectrum of myoglobin, which has no β-sheet secondary structures, shows that the amide I peak can have weaker absorption in the nominal "β-sheet" wavelength region of a simple model.

The new peak at $\sim$1743 cm^{-1} in the dying cell is usually associated with the non-hydrogen bonded ester carbonyl C=O stretching mode within phospholipids [25,36,61]. There is not a large increase in other lipid absorption bands in the dying cell, so this peak is not simply an increase in the number of lipid molecules or their density. A shoulder at $\sim$1725 cm^{-1} is also observed which is associated with hydrogen bonded C=O groups [25]. An increase in a peak at this position was seen by Jamin et al. [38], although in that study the authors investigated a cell which had experienced necrosis, and was visually changed morphologically due to a loss of cell membrane integrity [89]. When we investigated IMR-90 cells that had lost membrane integrity we observed similar results to those of Jamin et al. [38]. The fact that the $\sim$1743 cm^{-1} peak in Fig. 9 is significantly more intense than the $\sim$1725 cm^{-1} peak implies that the C=O ester carbonyl groups of lipids in the cell are becoming predominantly non-hydrogen bonded, which would be in agreement with the occurrence of oxidative damage. Apoptosis is associated with, among other factors, increased oxidative damage [4,55]. Therefore the cell we measured may be in the early stages of apoptosis and not a lysosomal type of death, whereas cells visually observed to have lost membrane integrity are most likely lysosomal and have different IR spectral characteristics.

It is also interesting to note that the peak at $\sim$1455 cm^{-1} becomes much sharper than was observed in any of the living cell cycle phase measurements. A vibration due to protein side chains is approximately at this position as well as some DNA/RNA and lipid vibrational modes. However, Venyaminov et al. [80] state that only pH or mutations can change vibrations from protein side chains. At present it is not clear which cellular component is causing this sharpened feature.

5. Cellular responses to dilute concentrations of TCDD

To compliment the above experiments following endogenous changes to living cells, we now turn to a health-related problem studying cellular responses to an exogenous environmental pollutant at realistic exposure concentrations [33]. Exposure to polychlorinated aromatic compounds (PAHs) can lead to various health effects including cancers, alteration of hormone levels, and reproductive defects in animals [9,17,43,56,81,86] and humans [26,29,40,44,59,60,63,79]. Among this family of pollutants, 2,3,7,8-tetrachlorodibenzo-p-dioxin (TCDD) is one of the most potent and most studied "man-made" toxins, causing harmful effects at exposure levels of hundreds or thousands of times lower than most chemicals of environmental concern [1]. As illustrated in Fig. 10, TCDD acts by binding to the aryl hydrocarbon (Ah) receptor [68,85]. Binding triggers induction of various genes involved in xenobiotic

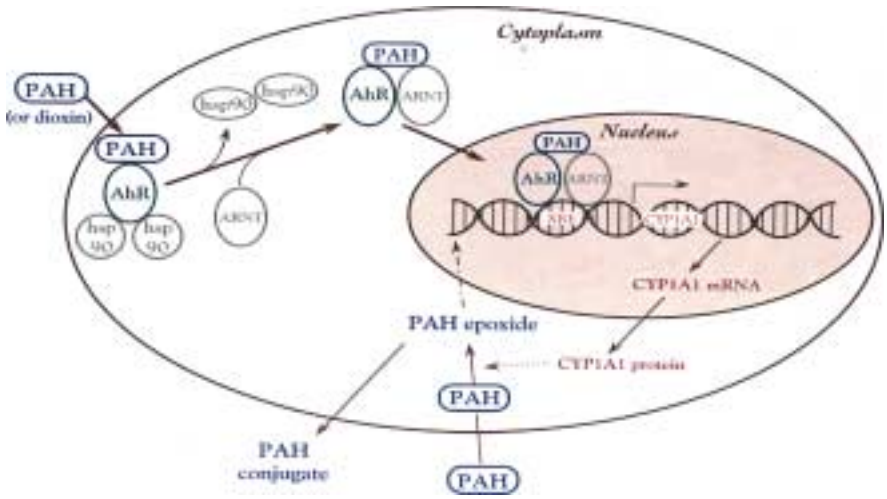

Fig. 10. Schematic diagram showing the human cellular response pathways for exposure to 2,3,7,8-tetrachlorodibenzo-p-dioxin (TCDD). This is also one of the response mechanisms to polycyclic aromatic hydrocarbons (PAHs). TCDD acts by binding to the aryl hydrocarbon (Ah) receptor which triggers induction of various genes involved in xenobiotic metabolism including the cytochrome P4501A1 (*CYP1A1*) gene. This gene codes for the CYP1A1 protein that metabolizes TCDD to water-soluble components that can be excreted from the cell. (Figure courtesy of Regine Goth-Goldstein.)

metabolism including the cytochrome P4501A1 (*CYP1A1*) gene [42,62,68,82,85]. TCDD was chosen for this study because the cellular response pathway is relatively straightforward and widely-studied, however there remain unresolved issues. For example, why is TCDD so much more toxic than other members of the same family of pollutants, even though a similar gene expression pathway is used? One widely-discussed explanation is that the presence of TCDD triggers methylation of the DNA and thus inhibits the expression of the CYP1A1 gene. In this study we use SR-FTIR spectromicroscopy to measure directly intracellular responses to TCDD, particularly the presence of methylation.

The SR-FTIR spectromicroscopy experiments began with exposing HepG2 cells (derived from a human hepatocellular carcinoma) to various dilute concentrations of TCDD. HepG2 cells were selected for use in this study as their ability to metabolize polyaromatic compounds is well characterized [22]. A fraction of the exposed cells were investigated by acquiring SR-FTIR spectra from individual live cells. The remaining cells were analyzed for *CYP1A1* gene expression, using the reverse transcriptase polymerase chain reaction (RT-PCR) technique. Observed changes in the SR-FTIR spectral measurements were compared with those from RT-PCR results.

As before, all SR-FTIR spectra were recorded in the 4000–650 cm^{-1} infrared region as this mid-IR region contains unique molecular absorption fingerprints, e.g., [45]. Every IR measurement consisted of 128 co-added spectra at a spectral resolution of 4 cm^{-1}. All spectra were obtained in the double-pass transmission geometry, were ratioed to the spectrum of a bare gold-coated slide, and absorbance values were computed. The center of each cell was found to within an accuracy of ± 2 μm by acquiring a line-map across each individual cell and then using the most absorbing, and therefore the thickest, part of the cell for analysis. Any residual water vapor features in the resultant spectrum were removed by subtracting an appropriately scaled reference spectrum of water vapor. To account for cell-to-cell thickness variations, the final spectrum from each cell was normalized with the protein amide II peak (1548 cm^{-1}) [57].

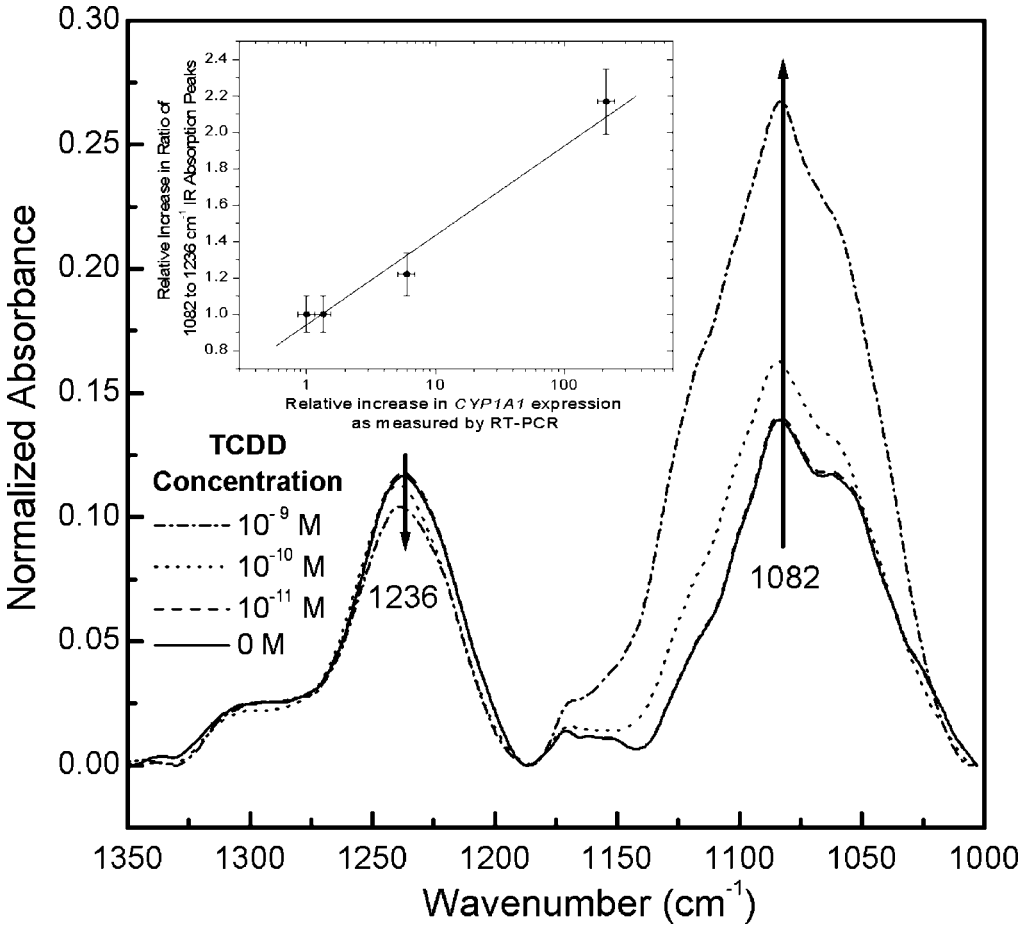

Fig. 11. Infrared spectra in the phosphate band region for cells treated with zero, 10^{-11}, 10^{-10}, and 10^{-9} molar TCDD. Spectra have been normalized to the protein amide II peak intensity to account for cell-to-cell thickness variations. The inset compares the ratio of these phosphate peaks and the CYP1A1 gene activity as measured by RT-PCR.

Figure 11 shows the IR spectra of unexposed HepG2 cells (solid line) and of cells exposed to different concentrations of TCDD in the phosphate band region. For untreated cells the phosphate absorption bands [61,66] at 1236 cm^{-1} (asymmetric phosphate stretching mode ν_{as} PO_2^-) and at 1082 cm^{-1} (symmetric phosphate stretching mode ν_s PO_2^-) were approximately equal in strength. For TCDD-treated HepG2 cells, the ν_{as} PO_2^- band decreased somewhat in intensity while the ν_s PO_2^- band increased by more than a factor of two for the highest TCDD doses studied. There were no detectable frequency shifts of either phosphate-stretching mode for TCDD treatments studied.

RT-PCR was carried out on extracts from the cell cultures of each TCDD exposure concentration. Measured values of *CYP1A1* gene expression were normalized to measured β-actin levels, and finally the relative increase in *CYP1A1* as a function of TCDD was obtained. The above systematic spectral changes obtained by SR-FTIR spectromicroscopy were compared with results from the RT-PCR technique. This comparison was done to determine if the SR-FTIR spectral changes could be associated with intracellular changes due to the induction of the *CYP1A1* gene. The relative increase in the ratio of the symmetric to asymmetric phosphate infrared bands with increasing TCDD concentration was compared to the relative

increase in *CYP1A1* induction in the inset to Fig. 11. Error bars for the IR data arose from the fact that we measured at 5 or less cells for each treatment concentration. The solid line in Fig. 7 is a weighted linear regression fit to the data. The excellent agreement (with $r^2 = 0.96$) for measurements from the two methods indicates that the rapid SR-FTIR spectromicroscopy technique can measure biochemical changes due to the *CYP1A1* expression processes.

Spectral absorption due to hydrocarbon vibrations in lipids, proteins, nucleic acids, sugars, and phosphates, among others were found within the 3050–2800 cm^{-1} region. Figure 12 displays the SR-FTIR spectra of unexposed HepG2 cells (solid line) and of cells exposed to different concentrations of TCDD in the C−H stretch region normalized to the peak maximum near 2925 cm^{-1}. The band near 2853 cm^{-1} is due to the symmetric CH_2 stretching mode of methylene groups; the peak at ∼2925 cm^{-1} is due to the asymmetric CH_2 stretch; the 2961 cm^{-1} absorption is due to asymmetric stretching of the CH_3 methyl groups; and the 2871 cm^{-1} mode is from the symmetric CH_3 stretching mode [66,71,86]. For TCDD-treated HepG2 cells, the 2853 peak decreased in intensity while the 2961 and 2871 cm^{-1} peaks increased. This indicates that the ratio of the number of methyl groups to that of methylene groups increases as the TCDD concentration increases. All C−H bands shown in Fig. 12 were observed to stiffen with increased TCDD exposure.

The relative change in intensities of the C−H stretching vibrations indicates that the number of methyl groups is increased compared to methylene groups upon exposure to TCDD. Other authors have proposed that TCDD removes the protection from methylation from certain sites when it binds to the Ah receptor [16], or increased methylation may down-regulate the expression of the *CYP1A1* gene [73].

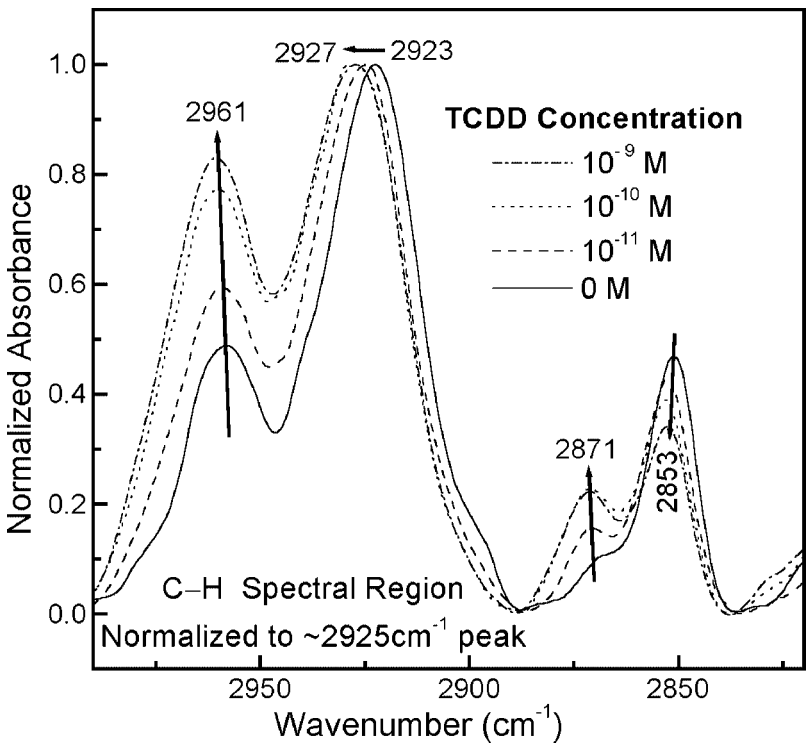

Fig. 12. Infrared spectra in the C–H stretching vibration region for cells treated with zero, 10^{-11}, 10^{-10}, and 10^{-9} molar TCDD. Spectra have been normalized to the ∼2925 cm^{-1} peak height. The peaks associated with methyl groups increase with TCDD concentration.

Since methylation is so intimately involved with gene inactivation [27], many have suggested that this increased methylation could explain the tremendous toxicity of TCDD in mammals. Our data, however, suggest that while increased methylation may be present CYP1A1 gene expression continues.

6. Conclusions

In summary, we have introduced the newly emerging synchrotron-based FTIR spectromicroscopy technique, shown that it is truly non-destructive for biological systems, and reviewed some early applications of the technique that serve to indicate the potential of the technique. Future work will build upon previous IR studies and complement other microscopy and biochemistry techniques to investigate changes in many different types of cells, as well as cellular biochemical processes resulting from a variety of agents. While the infrared spectra of whole cells are quite complex, the use of cell lines which are defective in a single process or pathway may allow the identification of key spectral features associated with important biochemical and physiological mechanisms. With sufficient development infrared spectromicroscopy may become a rapid and inexpensive diagnostic tool for medical screening applications. In addition, the single cell nature of the SR-FTIR technique will allow reliable detection and identification of a small number of cells within a sample that are different from the others, potentially opening new areas of research in environmental health and biomedicine.

The results reported here lay an important foundation for future biomedical and biological applications of synchrotron infrared spectromicroscopy, which will complement other biochemistry and microscopy techniques. SR-FTIR spectromicroscopy enables the successive monitoring of biochemical changes in individual cells non-destructively without having to treat cells with exogenous dyes, fluorescent labels, or stains, or to resort to destructive techniques. The non-invasive and non-destructive nature of the technique allows each cell in a population to be studied sequentially over a period extending to hours or even days. By monitoring individual cells over time it will be possible to detect the onset of disease and other cellular changes, and to probe the heterogeneity of responses to various treatments or insults within a population of living cells. The development of SR-FTIR spectromicroscopy will result in a broadly applicable and powerful research tool available to the scientific community.

Acknowledgements

This work was performed with support by the Directors of the Office of Science, Office of Biological and Environmental Research, Medical Science Division, the Office of National Petroleum Technology Program, the Office of Science, Basic Energy Sciences, Materials Science Division, of the United States Department of Energy under Contract No. DE-AC03-76SF00098, the Army Corps of Engineers of the U.S. Department of Defense, and the U.S. National Aeronautics Space Administration. This work could not have been accomplished without the invaluable contributions of Leonard Bjeldanes, Kathy Bjornstadt, Eleanor Blakely, Bruce Chase, John Crowe, Regina Goth-Goldstein, Terry Hazen, Jennie Hunter-Cevera, Kelly Knutsen, Morgan McNamara, Jacque Riby, Marion Russell, Richard Saykally, Sherry Seybold, Nelly Tsvetkova and Miqin Zhang.

References

[1] Health Assessment for 2,3,7,8-tetrachlorodibenzo-p-dioxin (TCDD) and Related Compounds, U.S. Environmental Protection Agency, 1997.

[2] G.W. Barendsen, C.J. Koot, G.R. Van Kersen, D.K. Bewley, S.B. Field and C.J. Parnell, The effect of oxygen on impairment of the proliferative capacity of human cells in culture by ionizing radiations of different LET, *International Journal of Radiation Biology and Related Studies in Physics, Chemistry and Medicine* **10** (1966), 317.
[3] W.M. Becker, J.B. Reece and M.F. Poenie, The world of the cell, Benjamin/Cummings, Menlo Park, Calif., 1996.
[4] R. Birge, E. Fajardo and B. Hempstead, in: *When Cells Die: A Comprehensive Evaluation of Apoptosis and Programmed Cell Death*, R.A. Lockshin, Z. Zakeri and J.L. Tilly, eds, Wiley-Liss, New York, 1998, pp. 347.
[5] E.A. Blakely, C.A. Tobias, T.C. Yang, K.C. Smith and J.T. Lyman, Inactivation of human kidney cells by high-energy monoenergetic heavy-ion beams, *Radiation Research* **80** (1979), 122.
[6] E.A. Blakely, P.Y. Chang and L. Lommel, Cell-cycle-dependent recovery from heavy-ion damage in G-1-phase cells, *Radiation Research* **104** (1985), S.
[7] E.A. Blakely, R.J. Roots, P.Y. Chang, L. Lommel, L.M. Craise, E.H. Goodwin, E. Yee, D.P. Dodgen and W.F. Blakely, Cell-cycle dependence of X-ray oxygen effect role of endogenous glutathione, NCI (National Cancer Institute) Monographs 1988, p. 217.
[8] E.A. Blakely, Cell inactivation by heavy charged particles, *Radiation and Environmental Biophysics* **31** (1992), 181.
[9] P.J.A. Borm, A.M. Knaapen, R.P.F. Schins, R.W.L. Godschalk and F.-J.V. Schooten, Neutrophils amplify the formation of DNA adducts by benzo(a)pyrene in lung target cells, *Environmental Health Perspectives* **105** (1997), 1089.
[10] S. Boydston-White, T. Gopen, S. Houser, J. Bargonetti and M. Diem, Infrared spectroscopy of human tissue. V. Infrared spectroscopic studies of myeloid leukemia (ML-1) cells at different phases of the cell cycle, *Biospectroscopy* **5** (1999), 219.
[11] F. Briki, B. Busson, L. Kreplak, P. Dumas and J. Doucet, Exploring a biological tissue from atomic to macroscopic scale using synchrotron radiation: Example of hair, *Cellular and Molecular Biology* **46** (2000), 1005.
[12] D.M. Byler and H. Susi, Examination of the secondary structure of proteins by deconvoluted Fourier-transform IR spectra, *Biopolymers* **25** (1986), 469.
[13] G.L. Carr, J.A. Reffner and G.P. Williams, Performance of an infrared microspectrometer at the NSLS, *Review of Scientific Instruments* **66** (1995), 1490.
[14] G.L. Carr, High-resolution microspectroscopy and sub-nanosecond time-resolved spectroscopy with the synchrotron infrared source, *Vibrational Spectroscopy* **19** (1999), 53.
[15] G.L. Carr, Resolution limits for infrared microspectroscopy explored with synchrotron radiation, *Review of Scientific Instruments* **72** (2001), 1613.
[16] F. Carrier, C.-Y. Chang, J.-L. Duh, D.W. Nebert and A. Puga, Interaction of the regulatory domains of the murine Cyp1a1 gene with two DNA-binding proteins in addition to the Ah receptor and the Ah receptor nuclear translocator (ARNT), *Biochemical Pharmacology* **48** (1994), 1767.
[17] K. Chaloupka, M. Steinberg, M. Santostefano, L.V. Rodriguez, L. Goldstein and S. Safe, Induction of Cyp1a-1 and Cyp1a-2 gene expression by a reconstituted mixture of polynuclear aromatic hydrocarbons in B6C3F1 mice, *Chemico-Biological Interactions* **96** (1995), 207.
[18] Y.-Y. Chang, Cell cycle, *Radiation Research* **146** (1996), 494.
[19] L.-P.I. Choo, D.L. Wetzel, W.C. Halliday, M. Jackson, S.M. Levine and H.H. Mantsch, In situ characterization of beta-amyloid in Alzheimer's diseased tissue by synchrotron fourier transform infrared microspectroscopy, *Biophysical Journal* **71** (1996), 1672.
[20] H.A. Crissman, Z. Darzynkiewicz, R.A. Tobey and J.A. Steinkamp, Correlated measurements of DNA, RNA and protein in individual cells by flow cytometry, *Science* (Washington, DC) **228** (1985), 1321.
[21] B. Czerniak, Z. Darzynkiewicz, F. Herz, R.P. Wersto and L.G. Koss, Flow cytometry in clinical oncology: Cell cycle and DNA ploidy in assessing tumor behavior, *Materia Medica Polona* **21** (1989), 3.
[22] C. Delescluse, N. Ledirac, G. De Sousa, M. Pralavorio, D. Botta-Fridlund, Y. Letreut and R. Rahmani, Comparative study of CYP1A1 induction by 3-methylcholanthrene in various human hepatic and epidermal cell types, *Toxicology In Vitro* **11** (1997), 443.
[23] A. Diaspro, Introduction to two-photon microscopy, *Microscopy Research and Technique* **47** (1999), 163.
[24] M. Diem, S. Boydston-White and L. Chiriboga, Infrared spectroscopy of cells and tissues: Shining light onto a novel subject, *Applied Spectroscopy* **53** (1999), 148A.
[25] H. Fabian, D. Chapman and H.H. Mantsch, in: *Infrared Spectroscopy of Biomolecules*, H.H. Mantsch and D. Chapman, eds, Wiley-Liss, New York, 1996, pp. 341.
[26] P.B. Farmer, O. Sepai, R. Lawrence, H. Autrup, P.S. Nielsen, A.B. Vestergard, R. Waters, C. Leuratti, N.J. Jones, J. Stone, R.A. Baan, J.H.M. Van Delft, M.J.S.T. Steenwinkel, S.A. Kyrtopoulos, V.L. Souliotis, N. Theodorakopoulos, N.C. Bacalis, A.T. Natarajan, A.D. Tates, A. Haugen, A. Andreassen, S. Ovrebo, D.E.G. Shuker, K.S. Amaning, A. Schouft, A. Ellul, R.C. Garner, K.H. Dingley, A. Abbondandolo, F. Merlo, J. Cole, K. Aldrich, D. Beare, E. Capulas, G. Rowley, A.P.W. Waugh, A.C. Povey, K. Haque, M. Kirsch-Volders, P. Van Hummelen and P. Castelain, Biomonitoring human exposure to environmental carcinogenic chemicals, *Mutagenesis* **11** (1996), 363.
[27] D. Freifelder and G.M. Malacinski, *Essentials of Molecular Biology*, Jones and Bartlett Publishers, Boston, 1993.

[28] J.T. Geller, H.Y. Holman, G. Su, M.E. Conrad, K. Pruess and J.C. Hunter-Cevera, Flow dynamics and potential for biodegradation of organic contaminants in fractured rock vadose zones, *Journal of Contaminant Hydrology* **43** (2000), 63.
[29] P. Gustavsson, R. Jakobsson, H. Johansson, F. Lewin, S. Norell and L.-E. Rutkvist, Occupational exposures and squamous cell carcinoma of the oral cavity, pharynx, larynx, and oesophagus: A case-control study in Sweden, *Occupational and Environmental Medicine* **55** (1998), 393.
[30] P.I. Haris and D. Chapman, Does Fourier-transform infrared spectroscopy provide useful information on protein structures?, *Trends in Biochemical Sciences* **17** (1992), 328.
[31] H.-Y.N. Holman, D.L. Perry, M.C. Martin, G.M. Lamble, W.R. McKinney and J.C. Hunter-Cevera, Real-time characterization of biogeochemical reduction of Cr(VI) on basalt surfaces by SR-FTIR imaging, *Geomicrobiology Journal* **16** (1999), 307.
[32] H.-Y.N. Holman, M. Zhang, R. Goth-Goldstein, M.C. Martin, M. Russell, W.R. McKinney, M. Ferrari and J.C. Hunter-Cevera, in: *Micro- and Nanofabricated Structures and Devices for Biomedical Environmental Applications II*, M. Ferrari, ed., SPIE Proceedings, Bellingham, WA, 1999, pp. 55.
[33] H.-Y.N. Holman, R. Goth-Goldstein, M.C. Martin, M.L. Russell and W.R. McKinney, Low-dose responses to 2,3,7,8-tetrachlorodibenzo-p-dioxin in single living human cells measured by synchrotron infrared spectromicroscopy, *Environmental Science and Technology* **34** (2000), 2513.
[34] H.-Y.N. Holman, M.C. Martin, E.A. Blakely, K. Bjornstad and W.R. McKinney, IR spectroscopic characteristics of cell cycle and cell death probed by synchrotron radiation based Fourier transform IR spectromicroscopy, *Biopolymers: Biospectroscopy* **57** (2000), 329.
[35] H.-Y.N. Holman, K.A. Bjornstad, M.P. McNamara, M.C. Martin, W.R. McKinney and E.A. Blakely, Synchrotron infrared spectromicroscopy as a novel bioanalytical microprobe for individual living cells: Cytotoxicity considerations, *Journal of Biomedical Optics* **7** (2002), in press.
[36] M. Jackson and H.H. Mantsch, in: *Infrared Spectroscopy of Biomolecules*, H.H. Mantsch and D. Chapman, eds, Wiley-Liss, New York, 1996, pp. 311.
[37] N. Jamin, P. Dumas, J. Moncuit, W.H. Fridman, J.L. Teillaud, G.L. Carr and G.P. Williams, Chemical imaging of nucleic acids, proteins and lipids of a single living cell. Application of synchrotron infrared microspectrometry in cell biology, *Cellular and Molecular Biology* **44** (1998), 9.
[38] N. Jamin, P. Dumas, J. Moncuit, W.-H. Fridman, J.-L. Teillaud, G.L. Carr and G.P. Williams, Highly resolved chemical imaging of living cells by using synchrotron infrared microspectrometry, *Proceedings of the National Academy of Sciences of the United States of America* **95** (1998), 4837.
[39] M.J. Janiak, D.M. Small and G.G. Shipley, Temperature and compositional dependence of the structure of hydrated dimyristoyl lecithin, *Journal of Biological Chemistry* **254** (1979), 6068.
[40] D.H. Kang, N. Rothman, M.C. Poirier, A. Greenberg, C.H. Hsu, B.S. Schwartz, M.E. Baser, J.D. Groopman, A. Weston and P.T. Strickland, Interindividual differences in the concentration of 1-hydroxypyrene-glucuronide in urine and polycyclic aromatic hydrocarbon-DNA adducts in peripheral white blood cells after charbroiled beef consumption, *Carcinogenesis* (Oxford) **16** (1995), 1079.
[41] K. Konig, Multiphoton microscopy in life sciences, *Journal of Microscopy* (Oxford) **200** (2000), 83.
[42] D.S. Lang, S. Becker, R.B. Develin and H.S. Koren, Cell-specific differences in the susceptibility of potential cellular targets of human origin derived from blood and lung following treatment with 2,3,7,8-tetrachlorodibenzo-p-dioxin (TCDD), *Cell Biology and Toxicology* **14** (1998), 23.
[43] B.M. Lee and P.T. Strickland, Antibodies to carcinogen-DNA adducts in mice chronically exposed to polycyclic aromatic hydrocarbons, *Immunology Letters* **36** (1993), 117.
[44] J. Lewtas, D. Walsh, R. Williams and L. Dodbias, Air pollution exposure-DNA adduct dosimetry in humans and rodents: Evidence for non-linearity at high doses, *Mutation Research* **378** (1997), 51.
[45] J. Liquier and E. Taillandier, in: *Infrared Spectroscopy of Biomolecules*, H.H. Mantsch and D. Chapman, eds, Wiley-Liss, New York, 1996, pp. 131.
[46] H.H. Mantsch and D. Chapman, *Infrared Spectroscopy of Biomolecules*, Wiley-Liss, New York, 1996.
[47] M.C. Martin and W.R. McKinney, in: *Applications of Synchrotron Radiation Techniques to Materials Science IV*, S.M. Mini, S.R. Stock, D.L. Perry and L.J. Terminello, eds, Materials Research Society, 1998, p. 11.
[48] M.C. Martin, N.M. Tsvetkova, J.H. Crowe and W.R. McKinney, Negligible sample heating from synchrotron infrared beam, *Applied Spectroscopy* **55** (2001), 111.
[49] W.R. McKinney, C.J. Hirschmugl, H.A. Padmore, T. Lauritzen, N. Andresen, G. Andronaco, R. Patton and M. Fong, in: *Accelerator-Based Infrared Sources and Applications*, SPIE, San Diego, CA, 1997, p. 59.
[50] W.R. McKinney, M.C. Martin, J.M. Byrd, R. Miller, M. Chin, G. Portman, E.J. Moler, T. Lauritzen, J.P. McKean, M. West, N. Kellogg, V. Zhuang, P.N. Ross, J.W. Ager, W. Shan and E.E. Haller, in: *Accelerator-Based Sources of Infrared and Spectroscopic Applications*, G.L. Carr and P. Dumas, eds, SPIE Proceedings, Denver, CO, 1999, p. 37.

[51] L.M. Miller, G.L. Carr, G.P. Williams and M.R. Chance, Synchrotron infrared microspectroscopy as a means of studying chemical composition at a cellular level, *Biophysical Journal* **72** (1997), A214.
[52] L.M. Miller, A.J. Pedraza and M.R. Chance, Identification of conformational substates involved in nitric oxide binding to ferric and ferrous myoglobin through difference Fourier transform infrared spectroscopy (FTIR), *Biochemistry* **36** (1997), 12 199.
[53] L.M. Miller, C.S. Carlson, G.L. Carr and M.R. Chance, A method for examining the chemical basis for bone disease: Synchrotron infrared microspectroscopy, *Cellular and Molecular Biology* (Noisy-Le-Grand) **44** (1998), 117.
[54] L.M. Miller, J. Tibrewala and C.S. Carlson, Examination of bone chemical composition in osteoporosis using fluorescence-assisted synchrotron infrared microspectroscopy, *Cellular and Molecular Biology* **46** (2000), 1035.
[55] R. Mittler, in: *When Cells Die: A Comprehensive Evaluation of Apoptosis and Programmed Cell Death*, R.A. Lockshin, Z. Zakeri and J.L. Tilly, eds, Wiley-Liss, New York, 1998, pp. 147.
[56] S. Nesnow, J.A. Ross, G.D. Stoner and M.J. Mass, Mechanistic linkage between DNA adducts, mutations in oncogenes and tumorigenesis of carcinogenic environmental polycyclic aromatic hydrocarbons in strain A/J mice, *Toxicology* **105** (1995), 403.
[57] D. Neumann, C.P. Schultz and D. Helm, in: *Infrared Spectroscopy of Biomolecules*, H.H. Mantsch and D. Chapman, eds, Wiley-Liss, New York, 1996, pp. 279.
[58] W.W. Nichols, D.G. Murphy, V.J. Cristofalo, L.H. Tiji, A.E. Greene and S.A. Dwight, Characterization of a new human diploid cell strain, IMR-90, *Science* **196** (1977), 60.
[59] O. Omland, D. Sherson, A.M. Hansen, T. Sigsgaard, H. Autrup and E. Overgaard, Exposure of iron foundry workers to polycyclic aromatic hydrocarbons: Benzo(a)pyrene-albumin adducts and 1-hydroxypyrene as biomarkers for exposure, *Occupational and Environmental Medicine* **51** (1994), 513.
[60] G. Pan, T. Hanaoka, Y. Yamano, K. Hara, M. Ichiba, Y. Wang, J. Zhang, Y. Feng, Z. Shujuan, D. Guan, G. Gao, N. Liu and K. Takahashi, A study of multiple biomarkers in coke oven workers: A cross-sectional study in China, *Carcinogenesis* (Oxford) **19** (1998), 1963.
[61] F.S. Parker, *Applications of Infrared Spectroscopy in Biochemistry, Biology, and Medicine*, Plenum Press, New York, 1971.
[62] A.R. Parrish, N.F. Alejandro, R.C. Bowes and K.S. Ramos, Cytotoxic response profiles of cultured renal epithelial and mesenchymal cells to selected aromatic hydrocarbons, *Toxicology In Vitro* **12** (1998), 219.
[63] F.P. Perera, D.L. Tang, J.P. O'Neill, W.L. Bigbee, R.J. Albertini, R. Santella, R. Ottman, W.Y. Tsai and C. Dickey, HPRT and glycophorin A mutations in foundry workers: Relationship to PAH exposure and to PAH-DNA adducts, *Carcinogenesis* (Oxford) **14** (1993), 969.
[64] T.K. Raab and M.C. Martin, Visualizing rhizosphere chemistry of legumes with mid-IR synchrotron radiation, *Planta* **213** (2001), 881.
[65] J.A. Reffner, P.A. Martoglio and G.P. Williams, Fourier transform infrared microscopical analysis with synchrotron radiation – the microscope optics and system performance, *Review of Scientific Instruments* **66** (1995), 1298.
[66] B. Rigas, S. Morgello, I.S. Goldman and P.T.T. Wong, Human colorectal cancers display abnormal Fourier-transform IR spectra, *Proceedings of the National Academy of Sciences of the United States of America* **87** (1990), 8140.
[67] M.J. Ruocco and G.G. Shipley, Characterization of the subtransition of hydrated DPPC bilayers. Kinetics, hydration and structural study, *Biochim. Biophys. Acta* **691** (1982), 309.
[68] S.H. Safe, Modulation of gene expression and endocrine response pathways by 2,3,7,8-tetrachlorodibenzo-p-dioxin and related compounds, *Pharmacology & Therapeutics* **67** (1995), 247.
[69] T.F. Slater, *Biochim. Biophys. Acta* **77** (1963), 383.
[70] J.M. Squirrell, D.L. Wokosin, J.G. White and B.D. Bavister, Long-term two-photon fluorescence imaging of mammalian embryos without compromising viability, *Nature Biotechnology* **17** (1999), 763.
[71] B. Stuart and D.J. Ando, Biological applications of infrared spectroscopy, Published on behalf of ACOL (University of Greenwich) by John Wiley, Chichester, New York, 1997.
[72] W.K. Surewicz and H.H. Mantsch, New insight into protein secondary structure for resolution-enhanced IR spectra, *Biochimica et Biophysica Acta* **952** (1988), 115.
[73] Y. Takahashi, C. Suzuki and T. Kamataki, Silencing of CYP1A1 expression in rabbits by DNA methylation, *Biochemical and Biophysical Research Communications* **247** (1998), 383.
[74] A.C. Thompson, J.H. Underwood, E.H. Anderson, S.A. McHugo and B.P. Lai, in: *Advances in X-Ray Optics*, A.K. Freund, T. Ishikawa, A.M. Khounsary, D.C. Mancini, A.G. Michette and S. Oestreich, eds, SPIE Proceedings, San Diego, CA, 2000, p. 16.
[75] U.K. Tirlapur, K. Koenig, C. Peuckert, R. Krieg and K.-J. Halbhuber, Femtosecond near-infrared laser pulses elicit generation of reactive oxygen species in mammalian cells leading to apoptosis-like death, *Experimental Cell Research* **263** (2001), 88.
[76] H. Torii and M. Tasumi, in: *Infrared Spectroscopy of Biomolecules*, H. Mantsch and D. Chapman, eds, Wiley-Liss, New York, 1996, p. 1.

[77] M. Tsuboi, S. Takahashi and I. Harada, in: *Physico-Chemical Properties of Nucleic Acids*, J. Duchesne, ed., Academic Press, London, New York, 1973, pp. 91.
[78] J. van der Veen, L. Bots and A. Mes, Establishment of two human cell strains from kidney reticulosarcoma of lung, *Arch. Ges. Virusforsch* **8** (1958), 230.
[79] F.J. Van Schooten, R.W.L. Godschalk, A. Breedijk, L.M. Maas, E. Kriek, H. Sakai, G. Wigbout, P. Baas, L. Van T Veer and N. Van Zandwijk, 32 P-postlabelling of aromatic DNA adducts in white blood cells and alveolar macrophages of smokers: Saturation at high exposures, *Mutation Research* **378** (1997), 65.
[80] S.Y. Venyaminov, W.D. Braddock and F.G. Prendergast, Infrared spectroscopy of proteins in aqueous solution, *Biophysical Journal* **70** (1996), A65.
[81] N.J. Walker, C.J. Portier, S.F. Lax, F.G. Crofts, Y. Li, G.W. Lucier and T.R. Sutter, Characterization of the dose-response of CYP1B1, CYP1A1, and CYP1A2 in the liver of female Sprague-Dawley rats following chronic exposure to 2,3,7,8-tetrachlorodibenzo-p-dioxin, *Toxicology and Applied Pharmacology* **154** (1999), 279.
[82] D. Warshawsky, G.K. Livingston, M. Fonouni-Fard and K. La Dow, Induction of micronuclei and sister chromatid exchanges by polycyclic and N-heterocyclic aromatic hydrocarbons in cultured human lymphocytes, *Environmental and Molecular Mutagenesis* **26** (1995), 109.
[83] D.L. Wetzel, J.A. Reffner and G.P. Williams, Synchrotron-powered FT-IR microspectroscopy: Single cell interrogation, *Mikrochimica Acta* (1997), 353.
[84] D.L. Wetzel and S.M. LeVine, Imaging molecular chemistry with infrared microscopy, *Science* (Washington DC) **285** (1999), 1224.
[85] J.P. Whitlock, Induction of cytochrome P4501A1, *Annual Review of Pharmacology and Toxicology* **39** (1999), 103.
[86] P.T.T. Wong, R.K. Wong, T.A. Caputo, T.A. Godwin and B. Rigas, Infrared spectroscopy of exfoliated human cervical cells: Evidence of extensive structural changes during carcinogenesis, *Proceedings of the National Academy of Sciences of the United States of America* **88** (1991), 10 988.
[87] A.H. Xie, Q. He, L. Miller, B. Sclavi and M.R. Chance, Low frequency vibrations of amino acid homopolymers observed by synchrotron far-IR absorption spectroscopy: Excited state effects dominate the temperature dependence of the spectra, *Biopolymers* **49** (1999), 591.
[88] D.K. Yip and N. Auersperg, The dye-exclusion test for cell viability: persistence of differential staining following fixation, *In Vitro* **7** (1972), 323.
[89] Z. Zakeri, in: *When Cells Die: A Comprehensive Evaluation of Apoptosis and Programmed Cell Death*, R.A. Lockshin, Z. Zakeri and J.L. Tilly, eds, Wiley-Liss, New York, 1998, p. 97.